Progress In Electromagnetics Research M, Vol. 98, 35–44, 2020

A New Passive Coding Imaging Method in Synthetic Aperture Interferometric Radiometer

Jinguo Wang*, Zhaozhao Gao, Jie Gu, Xiaoyun Zhang, Shiwen Li, Zitong Dong, Zilong Zhao, Fan Jiang, Bo Qi, and Wei Zhao

Abstract—Synthetic aperture interferometric radiometer (SAIR) is a high-resolution passive imager by sparsely arranging a number of small aperture antennas to synthesize a large aperture. However, the SAIR requires as many receivers as antennas needed, which results in high system complexity and hardware cost and limits the application of the SAIR. Aiming to reduce the system complexity of SAIR, a new passive coding imaging method is proposed in this paper. By using a new aperture coded measurement approach, the proposed method can significantly reduce the number of RF chains while keeping the image fidelity. The effectiveness of the proposed imaging method has been verified by simulations. The results reveal that the proposed method can be an efficient alternative for simplifying the architectures of SAIR.

1. INTRODUCTION

Synthetic aperture interferometric radiometer (SAIR) is a promising passive imager, which obtains brightness temperature (BT) images by measuring the objects natural radiation in the microwave band [1–8]. SAIR can realize high spatial resolution by using a thin array composed of numerous small aperture antennas to achieve a large aperture antenna and overcome the mechanical scan limitation of a traditional real aperture radiometer. Nevertheless, SAIR requires a large number of antennas and receivers to obtain as much information of the scene as possible, which results in increased system complexity and hardware cost and limits the applications of the SAIT in various domains.

In order to reduce the high complexity of a SAIR system, numerous researches have been performed. These developed methods can be summarized into three categories: one based on the clock scanning technique, one based on the compressed sensing (CS) technique, and one based on the passive coding technique. For example, Zhang et al. proposed a clock scan microwave interferometric radiometer (CSMIR) to reduce the complexity of the SAIR [7, 8]. However, the CSMIR requires the rotation equipment and is suitable for observing slow changing targets [8]. The CS approach reconstructs the BT images by randomly selecting partial visibility samples from all visibility samples. The feasibility of the CS method is demonstrated for reducing the complexity of the SAIR system [9, 10]. Kpré and Decroze proposed a passive coding technique to reduce the hardware cost of the SAIR system [11–13]. By using an oversized microwave cavity as the passive coding device, the BT image can be effectively recovered solely with a few receivers.

In this paper, we propose a new passive coding imaging method for SAIR to reconstruct the BT image. Different from the competing methods in [11–13], the proposed method employs a compact variable fiber delay line (VFDL) as the passive coding device to encode the signal received by the antenna array. Then the BT image can be reconstructed by decoding the coded signal and using the Fourier transform method. Since the passive coding device proposed in this paper is more compact than

Received 18 June 2020, Accepted 4 September 2020, Scheduled 29 October 2020

* Corresponding author: Jinguo Wang (wangjinguo09@126.com).

The authors are with the Science and Technology on Electronic Information Control Laboratory, the 29th Research Institute of China Electronics Technology Group Corporation, Chengdu, Sichuan, China.

that in [11–13], the proposed method is suitable for engineering application. Simulations are given to validate the feasibility of the proposed method.

This paper is organized as follows. In Section 2, the theory of the proposed method is described. In Section 3, the numerical simulations are carried out to validate the effectiveness of the presented method. Conclusions are drawn in Section 4.

2. THEORY OF THE NEW PASSIVE CODING IMAGING METHOD FOR SAIR

In this section, the new passive coding imaging method for SAIR is introduced. Fig. 1 shows the schematic of the SAIR system with a new passive coding device.

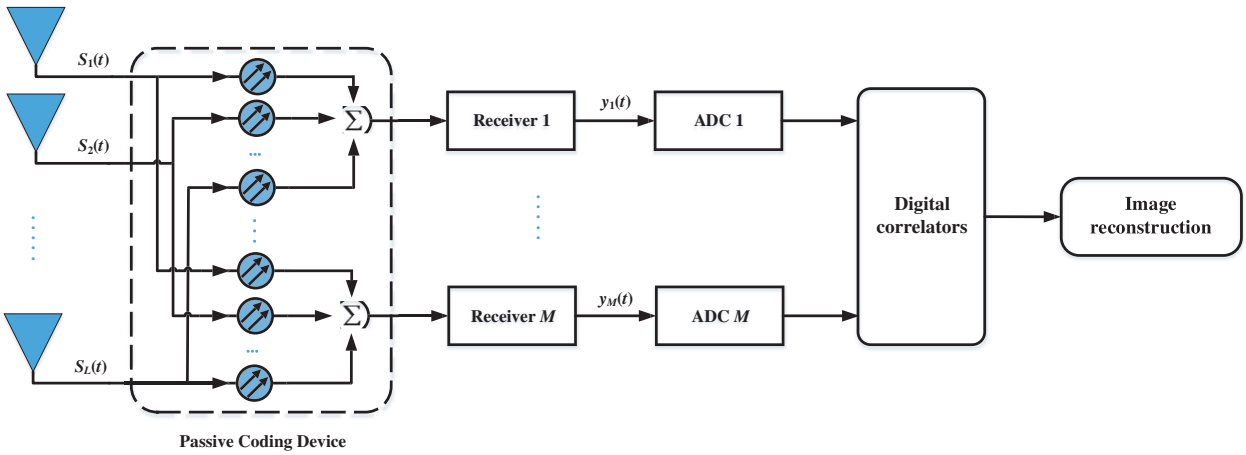

Figure 1. Schematic of the SAIR system with the new passive coding technique.

The receiving antenna array with L elements is connected to an $L\times M$ (Input/Output) ports passive coding device. The passive coding device, which consists of variable fiber delay lines (VFDLs), delays and multiplexes the received L antenna signals into M $(M<L)$ output signals, leading to architecture simplification. The data measured by receiver k in frequency domain are expressed as follows:

$$\begin{aligned} y_k(f) &= \sum_{l=1}^{L} h_{kl}(f)s_l(f) \\ &= \sum_{l=1}^{L} R_k(f)h'_{kl}(f)s_l(f) \end{aligned} \tag{1}$$

where $s_l(f)$ denotes the signal of interest received by the lth antenna, and $h_{kl}(f)$ is the transfer function between the lth antenna and the kth receiver. $R_k(f)$ and $h'_{kl}(f)$ are the transfer functions of the RF receiver and the passive coding device, respectively. The passive coding device shown in Fig. 1 is expressed as follows [11, 14]:

$$h_{kl}(t) = F\left[g_{kl}(t)e^{-i\omega(t-\tau_{kl})}\right] \tag{2}$$

where the symbol F denotes the Fourier transform, $g_{kl}(t)$ a random signal that obeys the random Gaussian distribution, and τ_{kl} the time delay between the lth antenna and the kth receiver.

Reformulating Eq. (1) into the matrix form:

$$y_k = \mathbf{h}_k\mathbf{s} \tag{3}$$

where $\mathbf{h}_k = [h_{k1}(f)\ h_{k2}(f)\ \ldots\ h_{kL}(f)] \in R^{1\times L}$, $\mathbf{s} = [s_1(f)\ s_2(f)\ \ldots\ s_L(f)] \in \mathbf{R}^{L\times 1}$.

Since the principle of the SAIR is to measure the cross correlation between each pair of the received signals $\mathbf{s}$, signals $\mathbf{s}$ should be estimated from the compressed data y_k for all frequency samples. According

to the CS theory [15], signals $\mathbf{s}$ can be recovered by solving the following convex optimization problem when it satisfies the sparse requirement, and $\mathbf{h}_k$ obeys the RIP condition [9, 10, 16],

$$\min \|\mathbf{s}\|_{l_1} \quad \text{s.t. } y_k = \mathbf{h}_k \mathbf{s} \tag{4}$$

Then the visibility samples of the observed scene can be computed by performing the cross correlation between each pair of the received signals $\mathbf{s}$:

$$V(u,v) = \left\langle s_i(f) \cdot s_j^*(f) \right\rangle \tag{5}$$

where the symbol $\langle \cdot \rangle$ denotes the inner product; $u = (x_i - x_j)/\lambda$, $v = (y_i - y_j)/\lambda$; λ is the wavelength; (x_i, y_i) and (x_j, y_j) are the positions of antennas i and j, respectively.

Based on the Van Cittert-Zernike theory, the brightness temperature (BT) image of the scene can be reconstructed by performing the inverse Fourier transform of the visibility samples [17]:

$$\begin{aligned} T(\xi,\eta) &= F^{-1}[V(u,v)] \\ &= \iint V(u,v) e^{j2\pi(u\xi+v\eta)} du dv \end{aligned} \tag{6}$$

where $(\xi, \eta) = (\sin\theta\cos\phi, \sin\theta\sin\phi)$.

From the above theoretical analysis, the proposed method has two constraints: the received signals should satisfy the sparsity in frequency domain, and the channels of the encoding device should satisfy the orthogonality constraint. Once these two conditions are met, the received signals $\mathbf{s}$ can be accurately estimated from the compressed data, and then the BT image of the scene can be reconstructed. Therefore, a key point of the proposed method in this paper is to design the time delay of the VFDLs to ensure that the channels of the encoding device satisfy the orthogonality constraint. The orthogonality constraint of the encoded device with the output port k can be evaluated by calculating the normalized correlation coefficients between the transfer functions of the passive coding device:

$$R_k = \mathbf{h}_k^H * \mathbf{h}_k \tag{7}$$

where $\mathbf{h}_k = [h_{k1}(f) h_{k2}(f) \dots h_{kL}(f)] \in \mathbf{R}^{1\times L}$.

When $R_k(i,i)$ tends to 1 and $R_k(i,j)$ tends to 0 $(i \neq j)$, the encoded device with output port k satisfies the orthogonality constraint. Therefore, the time delay of the VFDLs can be designed to ensure the encoded device satisfying the orthogonality constraints based on the above criteria.

3. NUMERICAL SIMULATIONS

In this section, several scenarios are shown to demonstrate the effectiveness of the proposed passive coding imaging method for reducing the system complexity while maintaining the image quality.

3.1. Case 1: SAIR System with a Circular Antenna Array

Firstly, the SAIR system with a circular antenna array is used to test the proposed method. The diameter of the circular antenna array is 7λ. 18 isotropic antennas are evenly arranged in the circular antenna array. The circular array configurations and their corresponding uv sampling grids are shown in Fig. 2(a) and Fig. 2(b), respectively. The uv sampling grids are denoted by the '$*$' symbol.

Then the proposed passive coding device with 18×4 ports is connected to the circular antenna array. According to the Eqs. (2) and (7), the normalized correlation coefficients between the transfer functions of the passive coding device can be calculated under the different lengths of VFDLs conditions. Based on the simulation results, the lengths of the VFDLs, which can make the channels of the encoded device satisfy the orthogonality constraints, are selected from a series of VFDLs with different lengths. In this case, the lengths of the VFDLs are set from 10 cm to 180 cm with an increase of 10 cm. Fig. 3 shows the normalized correlation coefficients between the transfer functions of the passive coding device with output port 1. From Fig. 3, the proposed passive coding device meets the non-correlation condition.

Figure 4(a) shows the original brightness temperature (BT) image of the scene. Two point-like targets with 300 K are set in the homogeneous background with 50 K. The targets are assumed to radiate the sinusoidal signals with central frequency of 1 GHz.

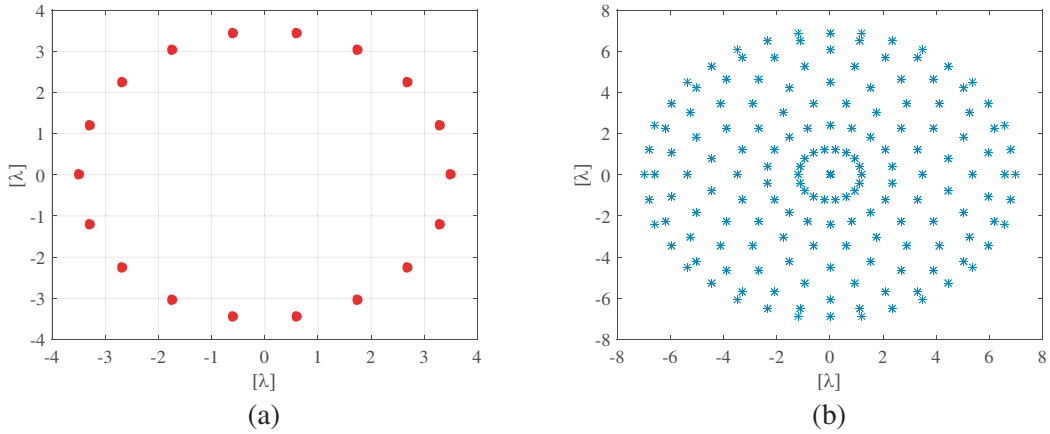

Figure 2. (a) Layout of the circular antenna array; (b) *uv* sampling grid coverage.

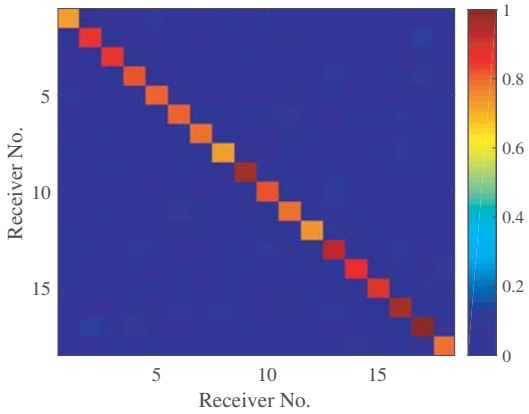

Figure 3. Normalized correlation coefficients between the transfer functions h_{1l}, $l \in [1, 2, \ldots, 18]$.

As a comparison, Fig. 4(b) shows the image reconstructed by the traditional SAIR system with the IDFT method. In the traditional SAIR system, each antenna is directly connected to a single receiver channel. The traditional SAIR system utilizes 18 antennas, 18 receivers, and 18 ADCs to reconstruct the image even though two targets are well recovered. Fig. 4(c) gives the result reconstructed by using the proposed passive coding imaging method solely with four receivers. Two targets are accurately reconstructed but with a few artifacts. In order to quantitatively compare the performance of different methods, the root mean square errors (RMSEs) of the results reconstructed by different methods are calculated according to the following equation:

$$\mathrm{RMSE} = \sqrt{\frac{1}{N}\sum_{n=1}^{N}(\mathbf{T}(n) - \mathbf{T}'(n))^2} \tag{8}$$

where T is the original BT image of the scene, T' the BT image reconstructed by the imaging method, and N the total pixel number of the BT image.

The RMSE in Eq. (8) denotes the error between the reconstructed image and the original image. The lower the RMSE is, the better the performance of the imaging method is. Based on Eq. (8), the RMSEs of Fig. 4(b) and Fig. 4(c) are 0.121 and 0.123, respectively. The proposed method has a similar imaging performance to the IDFT method while solely using 22% of the receivers employed by the IDFT method. The proposed method greatly reduces the hardware cost of the receiving chains in the SAIR system.

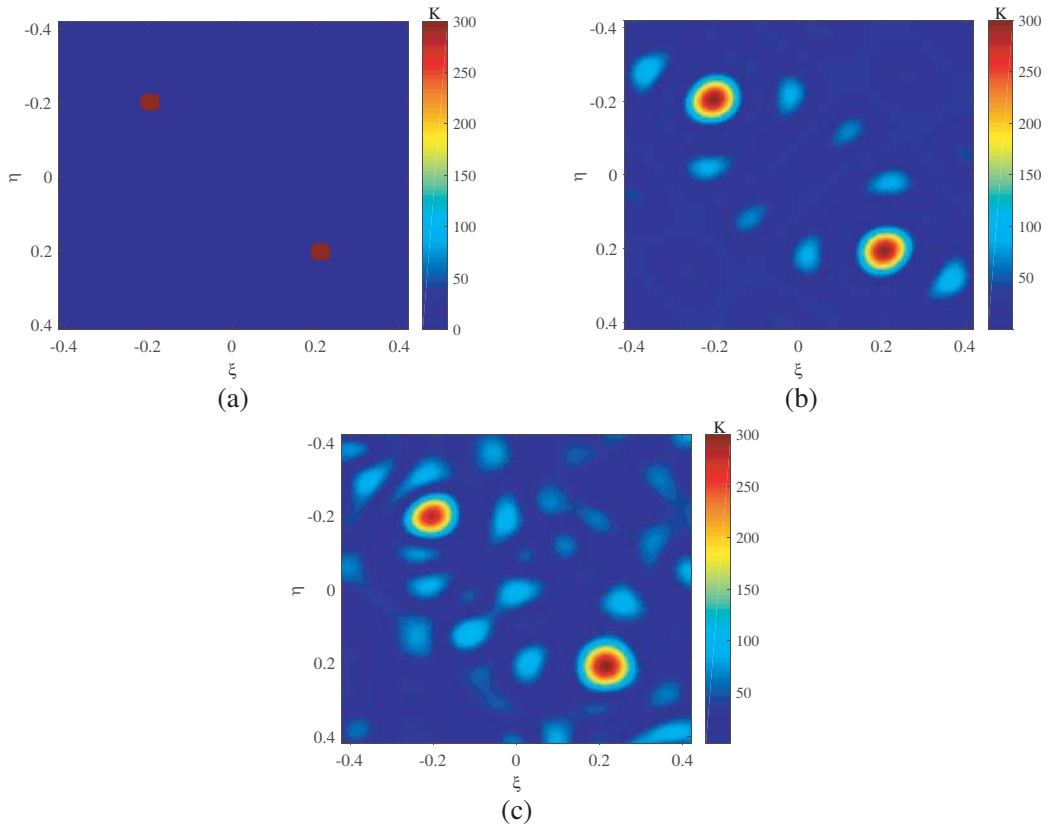

Figure 4. (a) Original image; (b) Image reconstructed by the traditional IDFT method with the circular antenna array and all 18 receivers; (c) Image reconstructed by the proposed method with the circular antenna array and 4 receivers.

3.2. Case 2: SAIR System with Y-Shaped Antenna Array

In the second case, a commonly used Y-shaped antenna array is used to test the efficiency of the proposed method. The Y-shaped antenna array consists of 24 isotropic antennas with equal space of 1.2λ. The configuration of the Y-shaped receiving array is shown in Fig. 5(a). Fig. 5(b) shows the uv sampling grid coverage of the Y-shaped antenna array.

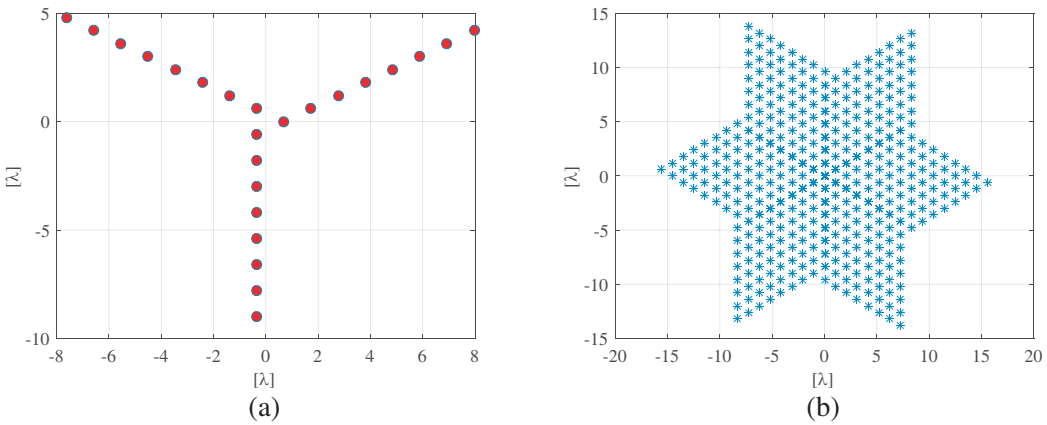

Figure 5. (a) Layout of the Y-shaped antenna array; (b) uv sampling grid coverage.

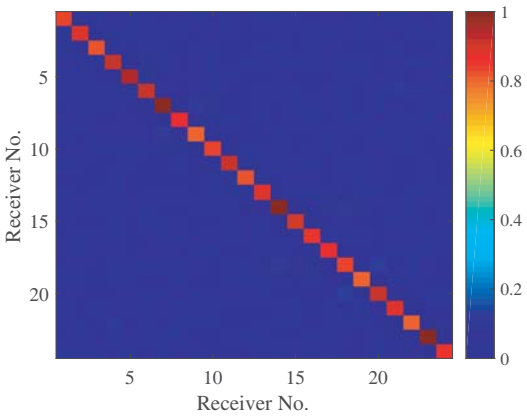

Figure 6. Normalized correlation coefficients between the transfer functions h_{1l}, $l \in [1, 2, \ldots, 24]$.

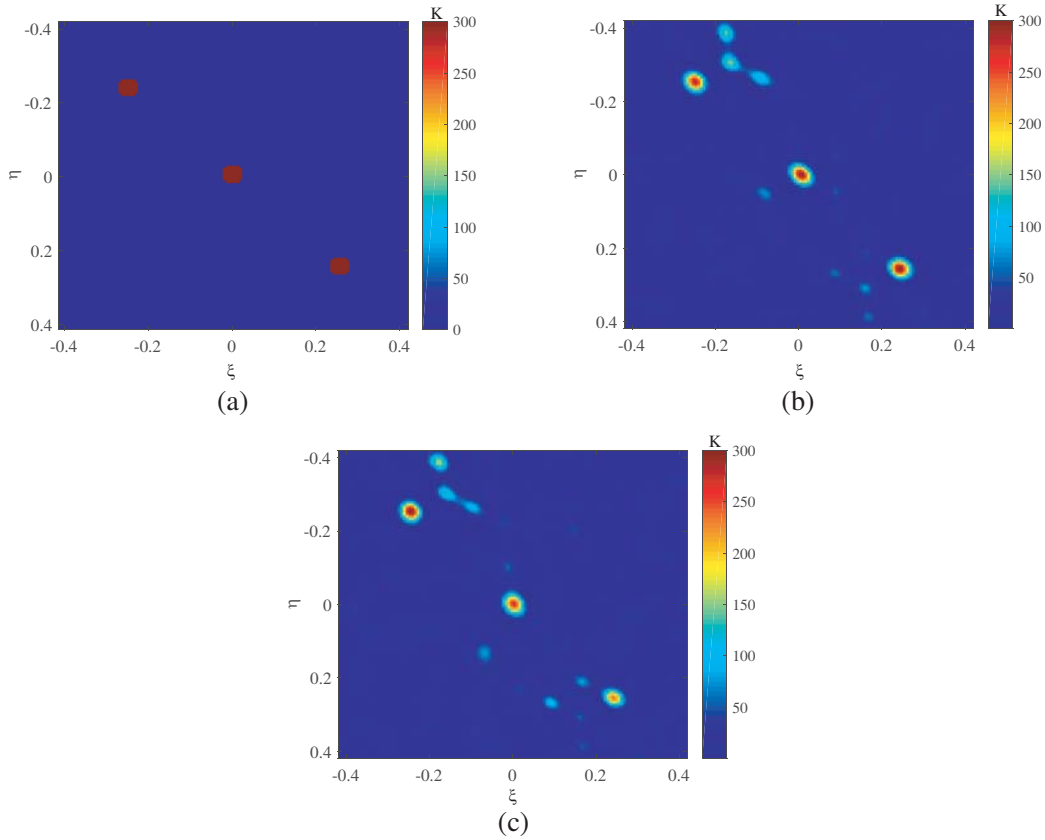

Figure 7. (a) Original image; (b) Image reconstructed by the IDFT method with the Y-shaped antenna array and all 24 receiver chains; (c) Image reconstructed by the proposed method with the Y-shaped antenna array and 4 receiver chains.

The passive coding device with 24×4 ports is connected to the Y-shaped antenna array shown in Fig. 5(a). The lengths of the VFDLs are set the same as those in the first case. Fig. 6 shows the normalized correlation coefficients between the transfer functions of the passive coding device. The proposed passive coding device satisfies the non-correlation constraint in this scenario.

With the proposed passive coding device, the data of the scene are compressively obtained by four receiver chains. Fig. 7(a) shows the original BT map of the scene. Three point-like targets with 300 K

are set in the homogeneous background with 50 K. The signals radiated by three targets are the same as those in the first case. Fig. 7(b) shows the image reconstructed by the traditional SAIR system with the IDFT method. Since the traditional SAIR system employs all 24 receivers to receive the data, three targets are accurately imaged. Fig. 7(c) shows the image reconstructed by using the proposed method solely with four receiver chains. Three targets are still well recovered but with the artifacts. The RMSEs of Fig. 7(b) and Fig. 7(c) are 0.102 and 0.107, respectively.

From Fig. 7, the proposed method has nearly the same imaging performance as the IDFT method while solely employing about 17% of the receiver chains used by the traditional IDFT method.

3.3. Case 3: T-Shaped Array

In this scenario, the SAIR system with the T-shaped antenna array is used to validate the proposed method. The T-shaped antenna array consists of 24 isotropic antennas with equal space of 1.2λ. The layout of the T-shaped antenna array is shown in Fig. 8(a). Fig. 8(b) shows the corresponding uv sampling grid coverage (denoted by the '$*$' symbol) of the T-shaped array.

A passive coding device, which is the same as that in case 2, is connected to the T-shaped antenna array. Fig. 9 shows the normalized correlation coefficients between the transfer functions of the passive coding device. From Fig. 9, the passive coding device meets the non-correlation constraint.

Figure 10(a) shows the original BT image of the simulated scene. Four point-like targets with 300 K are located in the homogeneous background. As a comparison, Fig. 10(b) shows the image reconstructed by the traditional SAIR system with the traditional IDFT method. Since the traditional IDFT method

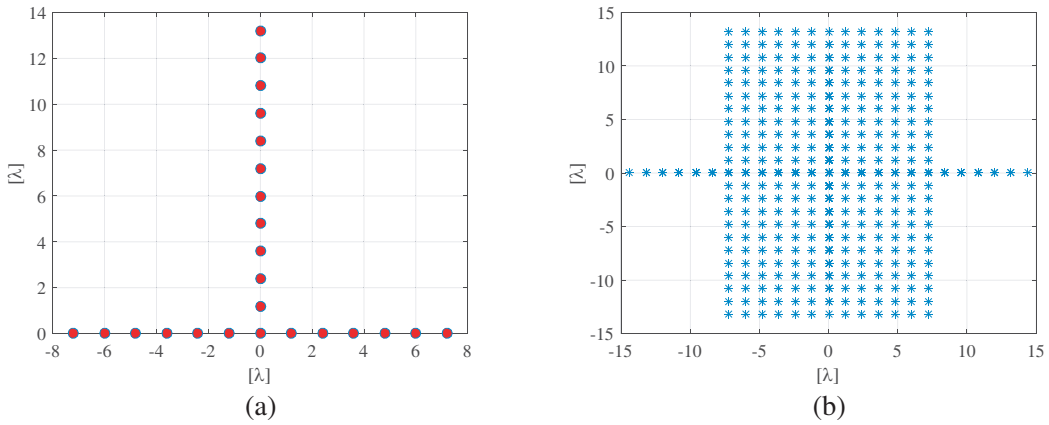

Figure 8. (a) Layout of the T-shaped antenna array; (b) uv sampling grid coverage.

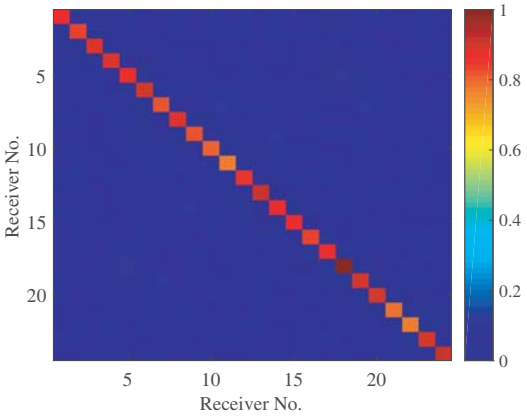

Figure 9. Normalized correlation coefficients between the transfer functions h_{1l}, $l \in [1, 2, \ldots, 24]$.

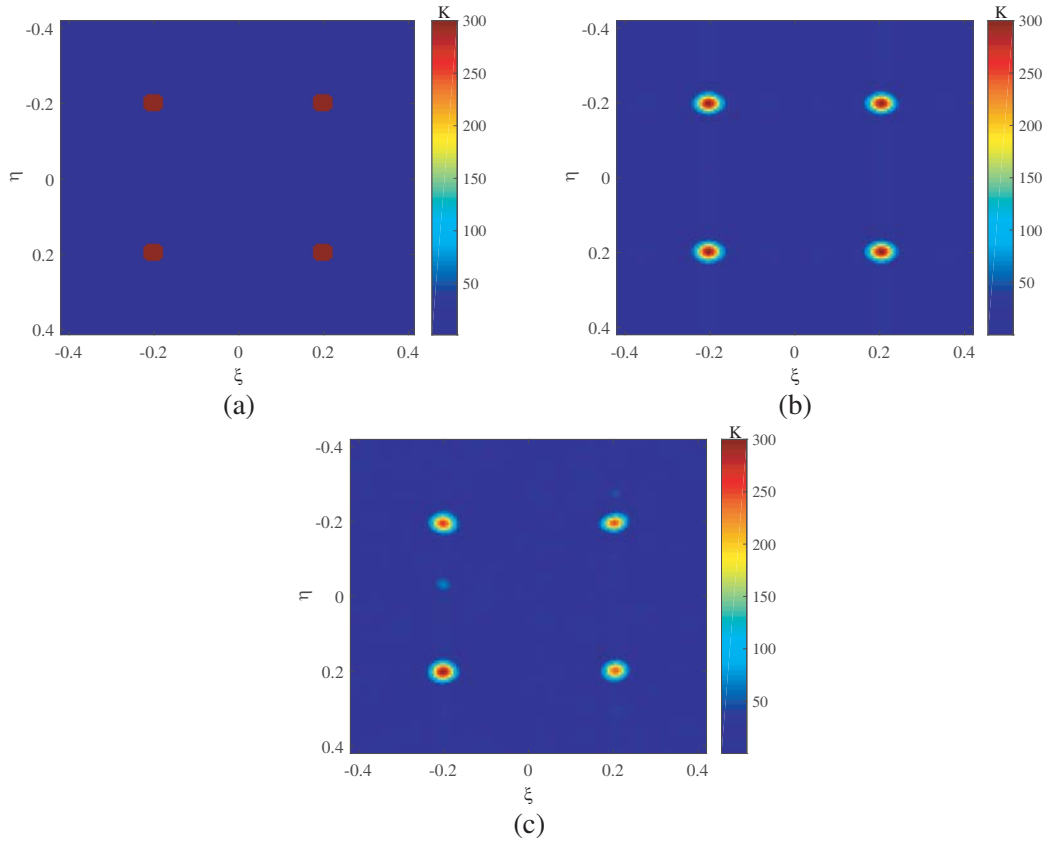

Figure 10. (a) Original image; (b) Image reconstructed by the IDFT method with the T-shaped antenna array and all 24 receivers; (c) Image reconstructed by the proposed method with the T-shaped antenna array and 4 receivers.

uses the samples obtained by all the receivers, four targets agree well with the original ones. Fig. 10(c) shows the image reconstructed by using the proposed passive coding imaging method. The RMSEs of Fig. 10(b) and Fig. 10(c) are about 0.095 and 0.108, respectively. The proposed method still recovers the targets with high fidelity solely with four receiver chains though the RMSE of the result imaged by the proposed method is a little higher than that imaged by the traditional IDFT method.

3.4. Case 4: Under the Noise Conditions

In the previous three examples, the validity of the proposed method has been demonstrated in different configurations of the antenna array without noise. In this case, the Gaussian noise will be contained in the simulated data to further test the performance of the proposed method.

The antenna array and the original BT image of the scene are set the same as those in case 1. Two point-like targets radiate sinusoidal signals with central frequency of 1 GHz. The signal is contaminated with Gaussian noise, and the SNR of the simulated data is about 10 dB.

Figure 11(a) shows the result reconstructed by the traditional SAIR system with the traditional IDFT method. The BT image of two targets is nearly the same as that in Fig. 4(b) even in the noise conditions. Fig. 11(b) shows the image reconstructed by using the proposed method with 6 receivers. A passive coding device with 18×6 ports is used in this case. The lengths of the VFDLs are the same as those set in case 1. Two targets are accurately reconstructed. Compared with the result in Fig. 4(c), two more receivers are used, and the artifacts are higher owing to the effect of the Gaussian noise. The RMSEs of the Fig. 11(a) and Fig. 11(b) are about 0.121 and 0.141, respectively, even though the RMSE of the image reconstructed by the proposed method is higher than that of the image reconstructed by the IDFT method.

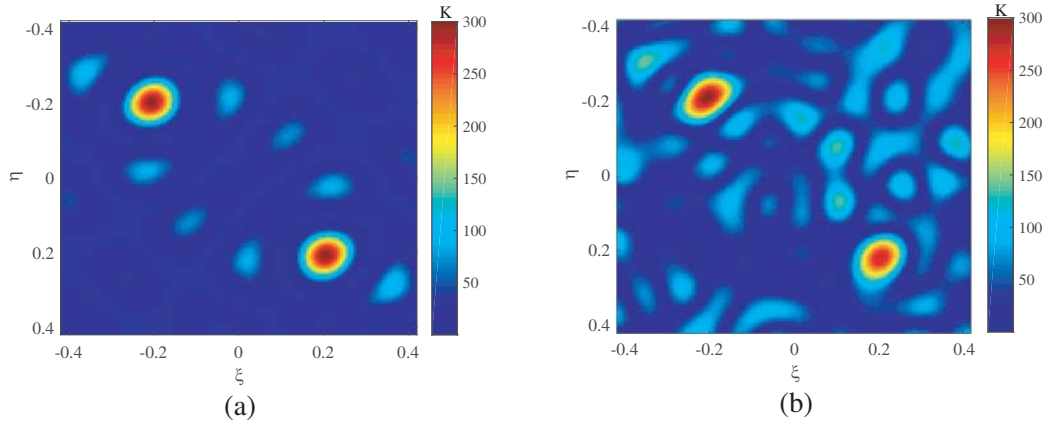

Figure 11. (a) Image reconstructed by the IDFT method with all 18 receivers; (b) Image reconstructed by the proposed method solely with 6 receivers.

Through the numerical simulations in this section, the effectiveness of the proposed method is verified for excessively reducing the hardware cost of the SAIR system while maintaining the image quality.

4. CONCLUSIONS

In this paper, a new passive coding imaging method is developed to simplify the architecture of the SAIR system. By adjusting the VFDLs in the passive coding device, the proposed method compresses the signals received by multiple antennas and then recovers the BT image by extracting the interaction between antennas from the encoded signals. Some numerical simulations are carried out to validate the feasibility of the developed method. Compared with the competing methods, the proposed method can effectively reduce the hardware cost of the SAIR system with good engineering realizability.

ACKNOWLEDGMENT

This work was supported by the Science and Technology on Electronic Information Control Laboratory.

REFERENCES

1. Corbella, I., F. Torres, A. Camps, A. Colliander, M. Martín-Neira, S. Ribó, K. Rautiainen, N. Duffo, and M. Vall-llossera, "MIRAS end-to-end calibration: Application to SMOS L1 processor," *IEEE Trans. Geoscience and Remote Sensing*, Vol. 43, No. 5, 1126–1134, 2005.
2. Su, K., W. Z. Liu, B. R. Barat, D. E. Gary, H. Z. Michalopoulou, and J. F. Federici, "Two dimensional interferometric and synthetic aperture imaging with a hybrid terahertz/millimeter wave system," *Applied Optics*, Vol. 49, No. 19, 13–19, Jul. 2010.
3. Zhang, C., J. Wu, H. Liu, and Y. Yan, "Imaging algorithm for synthetic aperture interferometric radiometer in near field," *Science China Technological Sciences*, Vol. 54, No. 8, 2224–2231, 2011.
4. Wu, J., C. Zhang, H. Liu, and J. Yan, "Performance analysis of circular antenna array for microwave interferometric radiometers," *IEEE Trans. Geoscience and Remote Sensing*, Vol. 55, No. 6, 3261–3271, 2017.
5. Chen, J., Y. Li, J. Wang, Y. Li, and Y. Zhang, "An accurate imaging algorithm for millimeter wave synthetic aperture imaging radiometer in near field," *Progress In Electromagnetics Research*, Vol. 141, 517–535, 2013.
6. Zhang, Y., Y. Li, S. Zhu, and Y. Li, "A robust reweighted L1-minimization imaging algorithm for passive millimeter wave SAIR in near field," *Sensors*, Vol. 15, No. 10, 24945–24960, Sept. 2015.

7. Zhang, C., H. Liu, L. Niu, and J. Wu, "System design and preliminary tests of an L-band clock scan microwave interferometric radiometer," *2017 International Geoscience and Remote Sensing Symposium*, 715–718, 2017.
8. Zhang, C., H. Liu, L. Niu, and J. Wu, "CSMIR: An L-band clock scan microwave interferometric radiometer," *IEEE Journal of Selected Topics in Applied Earth Observations and Remote Sensing*, 1–9, 2018.
9. Li, S., X. Zhou, B. Ren, H.-J. Sun, and X. Lv, "A compressive sensing approach for synthetic aperture imaging radiometers," *Progress In Electromagnetics Research*, Vol. 135, 583–599, 2013.
10. Wang, J., Z. Gao, J. Gu, S. Li, X. Zhang, Z. Dong, Z. Zhao, F. Jiang, B. Qi, and P. Xian, "A new passive imaging technique based on compressed sensing for synthetic aperture interferometric radiometer," *IEEE Geoscience and Remote Sensing Letters*, doi: 10.1109/LGRS.2019.2958033,
11. Kpré, E. L. and C. Decroze, "Passive coding technique applied to synthetic aperture interferometric radiometer," *IEEE Geoscience and Remote Sensing Letters*, Vol. 14, No. 8, 1193–1197, 2017.
12. Kpré, E. L. and C. Decroze, "Synthetic Aperture Interferometric Imaging using a passive microwave coding device," *2016 IEEE Conference on Antenna Measurements Applications (CAMA)*, 1–4, Oct. 23–27, 2016.
13. Kpré, E. L. and C. Decroze, "Passively coded synthetic aperture interferometric radiometer (CSAIR): Theory and measurement results," *European Conference on Antennas and Propagation*, 1243–1246, Mar. 23–27, 2017.
14. Hill, D. A., "Electromagnetic theory of reverberation chambers," *NIST Technical Note*, 1506, Dec. 1998.
15. Candes, E. J. and M. Wakin, "An introduction to compressive sampling," *IEEE Signal Processing Magazine*, Vol. 25, No. 2, 21–30, Mar. 2008.
16. Figueiredo, A. T., R. D. Nowak, and S. J. Wright, "Gradient projection for sparse reconstruction: Application to compressed sensing and other inverse problems," *IEEE Journal of Selected Topics in Signal Processing*, Vol. 1, No. 4, 586–597, 2007.
17. Hu, F., X. Peng, F. He, L. Wu, J. Li, Y. Chen, and D. Zhu, "RFI mitigation in aperture synthesis radiometers using a modified clean algorithm," *IEEE Geoscience and Remote Sensing Letters*, Vol. 14, No. 1, 13–17, 2017.